frontiers | Frontiers in Energy Research

TYPE Original Research
PUBLISHED 31 August 2022
DOI 10.3389/fenrg.2022.955465

OPEN ACCESS

EDITED BY
Greeshma Gadikota,
Cornell University, United States

REVIEWED BY
Jinze Xu,
University of Calgary, Canada
Hu Guo,
China University of Petroleum China

*CORRESPONDENCE
Lei Fu,
fulei@mail.cgs.gov.cn
Changyuan Zheng,
56295158@qq.com

SPECIALTY SECTION
This article was submitted to Carbon Capture, Utilization and Storage, a section of the journal Frontiers in Energy Research

RECEIVED 30 May 2022
ACCEPTED 25 July 2022
PUBLISHED 31 August 2022

CITATION
Fu L, Diao Y, Zheng C, Ma X, Zhang C, Liu T, Jin X and Shao W (2022), Caprock self-sealing effect due to CO_2 leakage from geologic carbon sequestration reservoirs: a case study at Ping'an, China.
Front. Energy Res. 10:955465.
doi: 10.3389/fenrg.2022.955465

Caprock self-sealing effect due to CO_2 leakage from geologic carbon sequestration reservoirs: a case study at Ping'an, China

Lei Fu[1]*, Yujie Diao[1], Changyuan Zheng[2,3]*, Xin Ma[1], Chenglong Zhang[1], Ting Liu[1], Xiaolin Jin[1] and Wei Shao[1]

[1]Center for Hydrogeology and Environmental Geology Survey, Baoding, China, [2]Qinghai Hydrogeology and Engineering Geology and Environgeology Survey Institute, Xining, China, [3]Hydrogeological and Geothermal Geological Key Laboratory of Qinghai Province, Xining, China

As a bottom technology for CO_2 reduction, geological CO_2 storage has attracted great attention from geologists, but there are few reports on the research of the caprock self-sealing effect due to CO_2 leakage. Ping'an is a natural CO_2 leakage site, which can be compared to the leakage scenarios of geological CO_2 storage. Based on the water quality test results and geological observation data, the numerical simulation of geochemistry is carried out. The results show that: First, gypsum dissolves and calcite precipitates during the migration of CO_2-rich water to the surface. This process presents a self-sealing effect, and the closer to the surface, the more obvious the self-sealing; Second, the self-sealing effect is formed rapidly. For a 30 cm wide fissure, it only takes a few hundred days to achieve self-sealing; Third, the CO2 leakage was estimated, about 140,813.3 m^3, or about 251.28 tons for 1 m long fissure.

KEYWORDS

geological CO2 storage, CO2 leakage, self-sealing, travertin, Ping'an

Introduction

Geological CO_2 storage (GCS) is considered to be an effective solution to alleviate global warming and environmental degradation because it can absorb greenhouse gases on a large scale (Jefferson, 2015). However, due to the complex deep geological conditions, unexpected geological events and human engineering activities, the risk of CO_2 leakage still exists (Xu et al., 2008). Potential leakage pathways for sequestered CO_2 include wells, faults, and "weak zones" in the caprock (Xie et al., 2017).

CO_2 leakage can cause serious geological environmental problems, such as the pollution of freshwater aquifers, and the enrichment of CO_2, which endangers nearby human health and local ecosystems (Cui et al., 2011; Jonathan et al., 2014; Ren et al., 2014; Taylor and Stahl, 2015; Vialle et al., 2016; Zhao et al., 2017; Zhai et al., 2018; Ma et al., 2020; Xiao et al., 2022). Many scholars have used a variety of methods to study the mechanism of CO_2 leakage and migration, the environmental impact and prevention measures. For example, Roberts has studied the relationship between the lithology,

structure and leak location of a natural CO_2 spring in Daylesford, Australia (Roberts et al., 2019). Ma D explored the identification method of geological CO_2 storage leakage based on neural network (Ma et al., 2020). Gal et al. studied CO_2 leakage and migration paths through controlled release experiments in shallow formations (Gal et al., 2013; Do et al., 2022; Melis et al., 2015; Schroder et al., 2017; Jones et al., 2014). Erik uses the method of analog gas well leakage to study the leakage path and leakage mechanism under the worst-case scenario of CO_2 geological storage (Erik et al., 2017). Mark L et al. studied the interception and accumulation effects of heterogeneous caprocks on CO_2 gas through laboratory experiments and numerical simulations (Mark et al., 2014; Ha et al., 2017; Saleem et al., 2021). Taking a natural CO_2 gas reservoir leaking site in South Africa as an object, Johnson used an analogy method to study the leakage of CO_2 geological storage along wells and faults (Johnson et al., 2017). Anelia et al. studied the effect of CO_2 leakage on the physical and chemical indicators of shallow aquifers (Susan et al., 2014; Qafoku et al., 2017; Choi, 2019; Delkhahi et al., 2020; Anelia et al., 2021). Li Xiaochun et al. used geomechanical modeling and numerical simulation to evaluate the sealing ability of caprock and the risk of fault activation in CO_2 storage sites (Li et al., 2003; Gale, 2004; Cui et al., 2011). Karas et al. introduced the repair measures and plugging effect of natural CO_2 gas reservoir leakage caused by blowout in Serbia (Karas et al., 2016). Zahasky C analyzes the feasibility of controlling reservoir pressure through injection-producer wells to stop CO_2 leakage (Zahasky and Benson, 2016).

Although many important achievements have been made in the migration path, environmental impact, and response measures of CO_2 geological storage leakage, the research on the self-sealing effect of CO_2 geological storage leakage are rarely reported. There are many natural CO_2 springs in Ping'an, which can be used to study the leakage scenarios of CO_2 geological storage by analogy. And there are many travertine platforms associated with the springs. The veins filled in the platform fissures provide a good research object for studying the self-sealing effect of CO_2 geological storage leakage.

Geological background

The study area is located in Ping'an County, Qinghai Province, China. The landform are mainly low mountains and hills, with an altitude of about 2400 m. The terrain is high in the south and low in the north. The tectonic structure is in the transition zone from the Loess Plateau to the Qinghai-Tibet Plateau. Affected by regional structure, it mainly develops two sets of faults. The NNE trending faults are extensional and torsional, and the NWW are compressional and torsional (Figure 1). Secondary tectonic units divided by faults have different hydrogeological conditions.

The structure of the study area is located in the Ping'an Sag of the Xining Basin. As a secondary structural unit of the Xining Basin, the Ping'an Sag has a deep basement and well-developed strata. The Proterozoic strata constitute the crystalline basement.

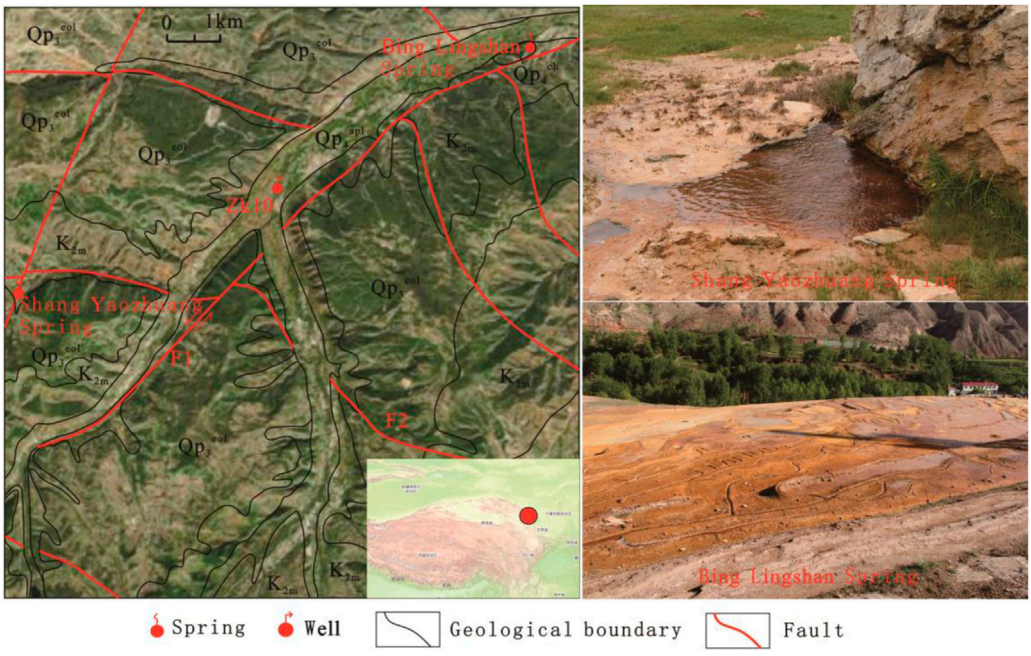

FIGURE 1
Geological scheme of the study area.

The upper strata are dominated by Mesozoic Cretaceous sandstone, glutenite and Cenozoic mudstone and siltstone. Quaternary aeolian, alluvial, ice-water deposits and a small amount of travertine deposits are widely distributed (Fu et al., 2019; Gupta and Yadav, 2020).

The Minhe Formation is mainly exposed in the study area, which is a lakeside sedimentary facies, and the lithology is mainly gypsum-bearing clastic rock. The lower part is dominated by conglomerate, which together with the underlying Early Cretaceous Estuary Group constitute the main reservoir in the region, with a thickness of 320.4–1,374.3 m. The upper part of the Minhe Formation is dominated by mudstone and silty mudstone, interspersed with fine sandstone and gypsum layers, with a thickness of 85.4–201.4 m, forming a regional caprock.

There are many natural CO_2 leakage points in the Ping'an area, including the Bing Lingshan spring, Shang Yaozhuang spring, and the ZK10 hole (Figure 1). Bing Lingshan spring is about 4.2 km northeast of Sanhe Town, with a water temperature of 19.5°C. There are sand gushing and bubbling in the spring, and a large thickness of travertine is developed. Shang Yaozhuang spring is about 6.4 km southwest of Sanhe Town, with a water temperature of 17.0°C. The spring is gushing sand and bubbling, and there is a large thickness of travertine around. ZK10 hole is located in the terrace of Qijiachuan Valley, 0.5 km southwest of Sanhe Town. It was the first time that high-pressure artesian water containing CO_2 gas was exposed in the Ping'an Sag. The depth of the well is 212.43 m, and the thickness of the aquifer containing CO_2 gas is 35.09 m. At the end of drilling in 2002, the water head was 73.00 m above the surface, and the artesian flow was 156.82 m^3/d. At present, the artesian flow has been greatly reduced, and it is speculated that the wellbore may be self-sealed by sediment. The well water temperature is 17.0°C, the salinity is 2.94 g/L, and the water chemical type is HCO_3·SO_4-Ca.

The ZK10 borehole is 212.43 m deep and mainly encounters the Minhe Formation (K2m). The 0–132.18 m stratum is dominated by brown-red mudstone, intercalated with thin layers of siltstone, which is a closed caprock for CO_2 sequestration; below 132.18 m is an interbed of gray-white fine sandstone and argillaceous sandstone, which contains water and gas, and is a CO_2 reservoir. When the borehole was drilled to 51 m, artesian water associated gas were found. After the drilling is completed, the still water level is 73 m above the surface. Under the premise that the reservoir is not exposed, water and gas are encountered in the closed caprock, indicating that the upper strata of the Minhe Formation have poor sealing performance. Under these conditions, deep CO_2 leaks to the surface in some way, as confirmed by a nearby natural CO_2 spring.

Methods and results

CO_2 source

The sources of CO_2 in groundwater can be roughly divided into organic and inorganic origins. Organic CO_2 mainly refers to the CO_2 produced by the decomposition of organic matter in the near-surface soil or by the respiration of plant roots. Inorganic CO_2 mainly related to deep metamorphism or magmatic activity, including the CO_2 produced by the pyrolysis of carbonate minerals, and the CO_2 carried in the hydrothermal fluid after the magmatic stage.

The origin of CO_2 can be identified according to $\delta^{13}C$, $^3He/^4He$ and R/Ra ($^3He/^4He$ ratio of sample to standard air). The $\delta^{13}C$ value of organic CO_2 is generally less than -10‰, and the R/Ra is less than 1. The $\delta^{13}C$ value of inorganic origin CO_2 is greater than 8‰. According to $^3He/^4He$ and R/Ra, inorganic CO_2 can be further divided into crust-derived type, mantle-derived type and mixed crust-mantle type. The $^3He/^4He$ of crust-derived type is low, and the R/Ra value is less than 1. The $^3He/^4He$ of mantle-derived type is high, and R/Ra is greater than 2. And the mixed crust-mantle type, due to the combined effect of the two factors, has an R/Ra value in the range of 1–2.

The gas composition and isotope analysis of typical CO_2 leakage sites in Ping'an are carried out, and the results are shown in Table 1. According to the results, the components in the gas sample are relatively simple, the main component is CO_2, and the content is more than 87.63%. Others are nitrogen, oxygen and trace argon, while hydrogen sulfide, hydrogen, methane and other alkanes were not detected. The $\delta^{13}C$ value of CO_2 gas reservoirs in the study area is -1.5‰ to -2.5‰, indicating that the CO_2 gas is inorganic origin. The lower values of $^3He/^4He$ and R/Ra indicate that the CO_2 gas lacks the participation of mantle fluids, which is a typical crust-derived type.

The study area is geothermally abnormal, and the distribution of numerous hot springs and high terrestrial heat flow also confirm the existence of deep heat sources. Therefore, it is speculated that the main source of CO_2 in the study area is the pyrolysis of deep carbonate in the crust.

Water chemistry

Water samples from natural CO_2 leak sites in the study area were tested for hydrochemistry. The water sample numbers of Bing Lingshan spring, Shang Yaozhuang spring and ZK10 boreholes are BLS, SYZ and ZK10 respectively. The water quality was analyzed by AT-510 automatic titration analyzer, and the results are shown in Table 2. The results show that SYZ and ZK10 have the same water chemical type, which is HCO_3·SO_4-Ca; and the water chemical type of BLS is HCO_3·SO_4-Na·Ca. Different hydrochemical types indicate that

TABLE 1 Gas composition and isotope analysis of CO_2 leakage points in the study area.

Serial number	T	Salinity (g/L)	pH	Main component (%)				$\delta^{13}C$ (‰)	Isotope ratio	
	(°C)			N_2	O_2	Ar	CO_2		$^3He/^4He$	R/Ra
BLS-1	19.5	5.47	6.54	4.59	1.4	0.067	93.95	−1.9	1.02×10^{-6}	0.73
BLS-2	19.5	5.47	6.54	4.44	1.35	0.067	94.14	−2.2	0.62×10^{-6}	0.44
SYZ	17	2.4	7.4	7.45	2.17	0.1	90.28	−2.5	1.42×10^{-6}	1.01
ZK10	17	2.94	6.63	9.66	2.58	0.13	87.63	−1.5	0.0626×10^{-6}	0.04

TABLE 2 Hydrochemical analysis of CO_2 leakage site.

Serial number	pH	T	Na^+	K^+	Ca^{2+}	Mg^{2+}	Fe^{3+}	Cl^-	SO_4^{2-}
		°C	mg/L	mg/L	mg/L	mg/L	mg/L	mg/L	mg/L
BLS	7.43	19.5	884.0	270.0	672.0	165.0	<0.04	295.0	1,478.0
SYZ	7.45	17.0	181.0	30.8	834.0	150.0	0.23	52.1	1,068.0
ZK10	7.28	17.0	281.0	121.0	805.0	165.0	0.05	69.5	908.0

Serial number	CO_3^{2-} mg/L	HCO_3^- mg/L	NO_3^- mg/L	F^- mg/L	H_2SiO_3 mg/L	Salinity mg/L	Free CO_2 mg/L	Water chemical type
BLS	0.0	3,293.0	0.14	0.52	12.7	2,358	16.4	HCO_3·SO_4-Na·Ca
SYZ	0.0	2,494.0	0.09	1.26	12.7	2,700	59.6	HCO_3·SO_4-Ca
ZK10	0.0	3,185.0	0.16	1.21	11.4	2,940	16.4	HCO_3·SO_4-Ca

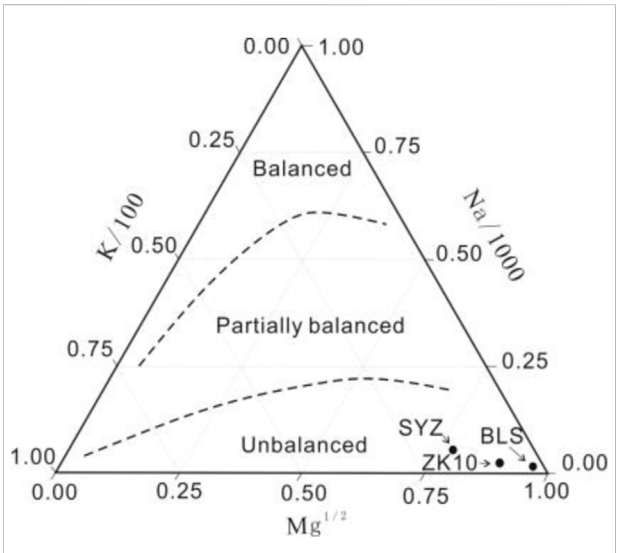

FIGURE 2
Na-K- Mg giggenbach plot with samples in the study area.

Bing Lingshan spring is in different hydrogeological units with ShangnYaozhuang spring and ZK10 borehole.

Plot the Na-K-Mg giggenbach diagram with the water chemistry data of the three samples to judge the equilibrium degree of the water-rock reaction (Figure 2). The results show that the three samples all fall in the unbalanced water area of the giggenbach diagram, indicating that during the migration of water along the fractures of the caprock to the surface, the dissolution and precipitation reaction will occur, which may promote the self-sealing of the caprock.

Microscopic morphology of veins

There are three forms of travertine. The first is the travertine veins developed in the bedrock strata; the second is the travertine platform cemented by the springs; the third is the chemical accumulation formed at the mouth of the hot spring and the wellhead of the geothermal well. The travertine veins filled in the fractures of the bedrock have the

FIGURE 3
Photo of travertine vein in Bing Lingshan.

deepest influence, and have the most significant influence on GCS.

The area of travertine in Bingling Mountain reaches 0.5 km^2. Affected by the uplift of neotectonic movement, the springs moved down to form three travertine platforms with a height difference of less than 30 m. The travertine platform is distributed in the SW-NE direction. The third-level platform in the SW direction is high and ancient, and the first-level platform in the NE direction is low and new. The third-level travertine platform is about 10 m thick, covered with Malan loess, and the lower stratum is Minhe Formation calcareous siltstone. The profile shows a number of vertical travertine veins, which are formed by the mineral precipitation in the original water-conducting fissures. It affirms the existence of the self-sealing effect of the caprock, and provides a good research target for studying the travertine self-sealing.

A typical travertine vein is selected for research (Figure 3). The thick of the vein is 24–30 cm, and can be divided into four layers from the center to the edge, representing four self-sealing stages. Described in order of formation time from late to early. The first layer is located in the middle of the vein, 6–8 cm thick, massive, uniform in texture, and earthy gray; the second layer is about 2 cm thick, in the shape of thin strips, including seven small laminae, alternating light and dark, with a single thin layer about 2 mm; the third layer is about 2–3 cm thick, massive, uniform in texture, light brown, with a longitudinal bright crystal calcite vein inside; the fourth layer is about 1–4 cm thick, in the shape of thin strip, including six small laminae, with a single layer thickness of 1–2 mm.

The vein The SEM photos of BLS01 and BLS02 are shown in Figure 4. BLS01 has a uniform structure, mainly composed of calcite and quartz. The sediment has a large particle size and a low clay content. It is speculated that the provenance was abundant and the deposition was rapid. BLS02 shows the contact relationship of laminae. The two sides are mainly calcite. The contact zone is composed of gypsum, biotite and illite. It is speculated that the two sides of the contact surface were formed in different stages. The small particle size of the sediment and the high content of clay minerals indicate that the sedimentation process was slow, the provenance was few and unstable.

REE in travertine

Travertine veins are the product of the interaction between fluid and deep fractured rock mass. It reflects the chemical composition of groundwater and is used to analyze the source of water supply. It can also reflect the temperature and pressure

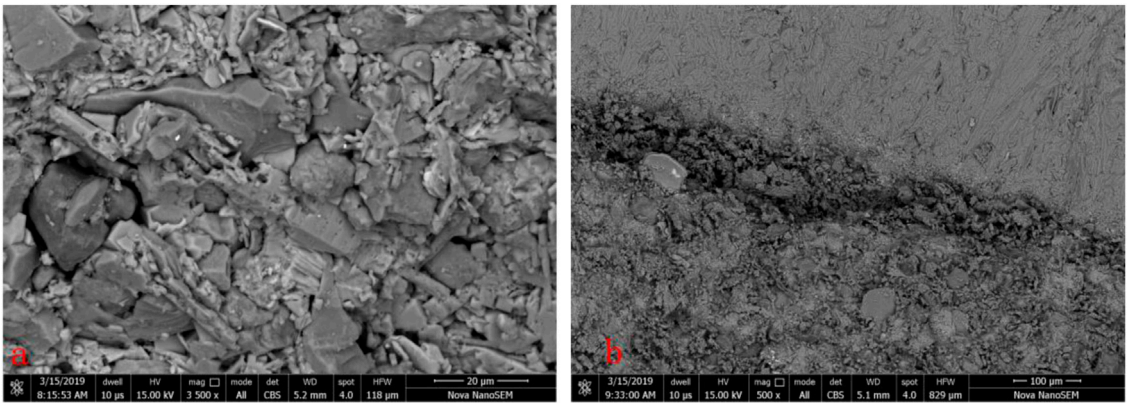

FIGURE 4
The SEM photos of BLS01**(A)** and BLS02 **(B)**.

conditions and surrounding rock information of the fracture system.

As a special element, rare earth elements (REE) occupy an important position in geochemical research. Because of their similar chemical properties, they coexist in nature, but there are slight differences in atomic structure, resulting in certain differences in the chemical properties of each element. Therefore, REE can undergo a certain fractionation in different geological processes, resulting in their distribution patterns with different characteristics. Based on this, according to the content data of REE in rocks and minerals, the chemical composition of the ancient fluid medium, the characteristics of the source area and the regional evolution history can be discussed.

REE analysis was carried out on the four travertine samples (Tables 3, 4), and the chondrite standard spider diagram and NASC normalized patterns were drawn as shown in Figures 5, 6. According to the distribution pattern of REE, the samples can be divided into two groups, BLS01 and BLS03 as a group, and BLS02 and BLS04 as a group. This result is consistent with the morphology of travertine, indicating that BLS01 and BLS03, BLS02 and BLS04 samples have different material sources and formation processes.

Numerical simulation

PHREEQC software was used for simulation. It is a powerful hydrogeochemical simulation software developed by the US Geological Survey and widely used in the field of hydrogeology. It is based on the water chemistry model of ionic connection, which can simulate reversible reactions such as mineral dissolution and precipitation, surface complexation, ion exchange, and irreversible reactions such as mixing with solution and redox. It can also do reverse modeling and find that minerals and gases transfer in water with indeterminate compositions. This software can simulate the mineral dissolution and precipitation reaction caused by pressure reduction and CO_2 overflow during the migration of CO_2-rich fluid to the surface, and is suitable for the study of self-sealing of CO_2 geological storage.

A conceptual model was established based on the vein body shape of the travertine platform in Bing Lingshan and the strata of the ZK10 borehole (Figure 7). The caprock is 200 m thick, and the lower part is a confined aquifer containing CO_2 gas. The fissure is 0.3 m wide and runs through the caprock longitudinally. The pressure at the bottom of the fissure is 28 atm, gradually reaching 1 atm to the surface, and the CO_2-rich fluid migrates from the reservoir to the surface along the fissure, and finally emerges into a spring. The fluid in the reservoir is in the supersaturated state of CO_2, and the main water quality ion indicators are set according to the ZK10 borehole water quality analysis results. The main ionic components are shown in Table 5.

CO_2 partial pressure and temperature have no effect on the reaction of feldspar and clay minerals, but these factors have a great influence on the reaction of calcite and gypsum. In this study, only calcite and gypsum were considered. The temperature of the fluid from the reservoir to the surface changes little, and only the effect of pressure on the solubility of CO_2 is considered. In the process of fluid migration to the surface, the single-width flow rate of fluid is set to 2 L/s, and the fluid is in equilibrium with the calcite and gypsum in the caprock.

The simulation results are shown in Figure 8. In the figure, it can be seen that gypsum dissolves and calcite precipitates during the migration of CO_2-rich water to the surface, and the closer to the surface, the greater the rate of dissolution and precipitation. During this process, the volume of precipitated calcite is larger than that of dissolved gypsum, and the overall performance is self-sealing of fissures, and the closer to the surface, the more obvious the self-sealing phenomenon.

Discussion

CO_2 leakage mechanism in Qinghai Ping'an

There are two sets of faults in the study area. The NNE-trending extensional faults have water-conducting properties, and the NWW-trending faults have water-blocking properties.

TABLE 3 Chemical analysis results of travertine samples.

Serial number	Si_2	Al_2O_3	Ti_2	Fe_2O_3	FeO	CaO	MgO	K_2O	Na_2O	MnO	P_2O_5	H_2O^+	H_2O^-	Loss on ignition	Sum
	%	%	%	%	%	%	%	%	%	%	%	%	%	%	%
BLS01	17.22	4.08	0.19	1.16	0.27	40.56	1.22	0.88	0.53	0.031	0.050	1.41	0.66	33.55	99.76
BLS02	9.68	2.47	0.11	0.83	0.26	46.81	0.72	0.52	0.44	0.016	0.033	1.41	0.77	37.77	99.64
BLS03	12.34	3.81	0.17	1.33	0.17	43.63	1.19	0.82	0.54	0.027	0.040	1.57	0.99	35.65	99.70
BLS04	4.91	1.53	0.06	1.84	0.16	50.39	0.61	0.34	0.35	0.029	0.027	1.66	1.06	39.37	99.61

TABLE 4 Trace elements analysis of travertine samples.

Serial number	μg/g																								
	Li	Be	Sc	V	Cr	Co.	Ni	Cu	Zn	Ga	Ge	Rb	Sr	Zr	Nb	Y	La	Ce	Pr	Nd	Sm	Eu	Gd		
BLS01	19.8	3.03	6.38	37.9	33.5	8.51	28.2	8.84	48.2	5.65	1.10	87.2	2,494	46.1	5.01	13.5	13.6	20.5	2.59	10.1	2.16	0.68	2.06		
BLS02	13.2	3.91	4.62	21.7	19.4	5.52	19.7	5.29	35.7	3.11	0.77	49.3	3,245	33.8	2.71	23.4	9.39	17.8	1.94	8.58	2.20	0.67	2.48		
BLS03	20.1	3.55	6.14	34.1	24.2	7.16	27.4	8.18	48.1	5.01	1.26	79.9	2,969	45.1	4.05	12.6	11.6	22.6	2.22	8.95	1.88	0.46	1.80		
BLS04	9.85	7.20	3.84	15.7	12.9	7.58	25.2	2.90	55.5	1.96	0.79	32.1	3,471	24.9	1.51	28.0	6.02	11.0	1.31	6.15	1.90	0.57	2.54		

Serial number	μg/g																					
	Tb	Dy	Ho	Er	Tm	Yb	Lu	Mo	Cd	In	Cs	Ba	Hf	Ta	W	Tl	Pb	Bi	Th	U	LREE/HREE	δEu	δCe
BLS01	0.36	2.10	0.40	1.08	0.18	1.02	0.16	0.51	0.23	0.022	11.49	177	1.15	0.32	0.61	0.97	8.66	0.11	3.73	14.4	6.74	0.98	0.77		
BLS02	0.48	3.11	0.61	1.58	0.25	1.35	0.22	0.20	0.11	0.013	6.89	144	0.68	0.19	0.36	0.60	6.58	0.063	2.26	30.1	4.03	0.88	0.94		
BLS03	0.32	1.92	0.37	1.00	0.16	0.92	0.15	0.29	0.18	0.020	11.28	208	0.87	0.27	0.55	0.84	7.91	0.12	3.50	21.8	7.19	0.76	0.99		
BLS04	0.52	3.52	0.71	1.86	0.28	1.44	0.22	0.23	0.070	0.009	4.57	97.9	0.45	0.13	0.25	0.52	5.31	0.043	1.52	30.7	2.43	0.80	0.89		

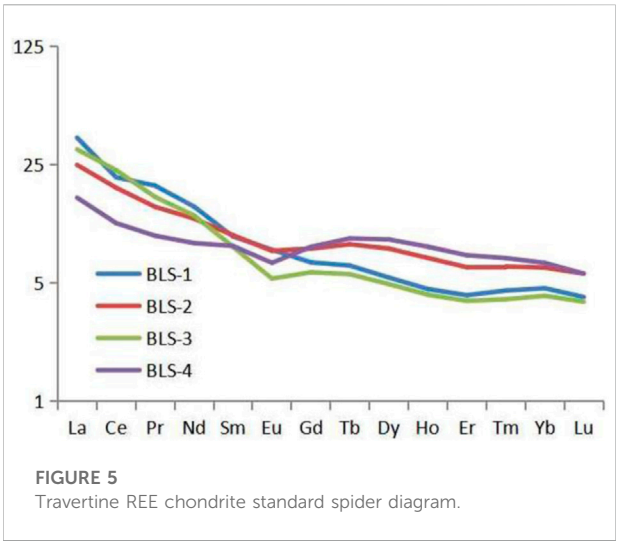

FIGURE 5
Travertine REE chondrite standard spider diagram.

NNE-trending extensional faults are developed along Qijiachuan (F1), and the outcropping lithology of the mountains on both sides of the fault is different. On the west side, the upper part of the Minhe Formation is exposed with fine-grained mudstone mixed with gypsum, which is a relatively descending depression; and on the east side, the coarse-grained strata in the lower part of the Minhe Formation is exposed, which is a relatively rising bulge. A south-dipping compressional fault (F2) is developed near the east-west direction on the south side of Sanhe Town. The study area is divided into checkerboard-like structural units by two sets of faults. In addition, on the north side of the F2 fault, there is an open syncline structure with an axial distribution in a near-north-south direction and the hub dipping to the north. The ZK10 borehole is located in good structural sealing conditions, with sufficient groundwater recharge source and good fault water storage structure. At the same time, the syncline structure and groundwater runoff also easily promote the migration and accumulation of CO_2 to the two flanks of the syncline structure, and then leak into spring along the fault.

The ZK10 borehole has intermittent CO_2 self-spraying phenomenon during construction. The eruption period is about 10 min, and the self-spraying duration is 210 s. The maximum instantaneous self-spraying water volume is 5835 m^3/d. The reason for this phenomenon is presumed that deep CO_2 migrates upwards into the reservoir through deep and large faults, and is blocked by the caprock. When the position is affected by the pressure reduction and volume expansion, the self-spray phenomenon occurs. The reason for this phenomenon is speculated to be that deep CO_2 migrated upward into the reservoir through deep and large faults. Prevented by the caprock, CO_2 accumulates on top of the reservoir. CO_2 migrates with the groundwater in the reservoir, and when it

migrates to the wellbore position, a self-spray phenomenon occurs, which is affected by pressure reduction and volume expansion.

Based on the above, there are three leakage channels in natural CO_2 gas reservoirs in the study area, including drilling holes, faults, and the "weak caprock zone" verified by hole ZK10. The natural CO_2 leakage mechanism in the study area is as follows: the deep carbonate minerals in the crust are decomposed at high temperature to generate CO_2, and the generated CO_2 rises into the reservoir along with the deep and large fault. Blocked by the caprock, CO_2 accumulates at the top of the reservoir, and then migrates to the above leakage channel with the groundwater flow, and finally leaks to the surface (Figure 9).

Self-sealing effect due to CO_2 leakage

Travertine self-sealing refers to the hydrothermal alteration or precipitation of minerals contained in underground hot water in some previously uncapped reservoirs, which can transform the overlying high-permeability geological structures into low-permeability ones. The formed travertine cemented rock layer can act as a caprock due to its low permeability, isolating the deep fluid from the surface.

The formation of travertine is mainly because the partial pressure of CO_2 in the water is higher than surrounding atmosphere, so that CO_2 escapes from the water, and the carbonate in the water is supersaturated and precipitated. The reaction formula of travertine formation is shown in Eq. 1.

$$Ca^{2+} + 2HCO_{3^-} \Leftrightarrow CaCO_3 \downarrow + CO_2 \uparrow + H_2O \qquad (1)$$

The chemical precipitation in Bing Lingshan spring is obvious, indicating that Ca^{2+} and HCO_3- in groundwater are in a supersaturated state. Due to the change of pressure, the leakage channel of CO_2 meets the conditions of travertine self-sealing.

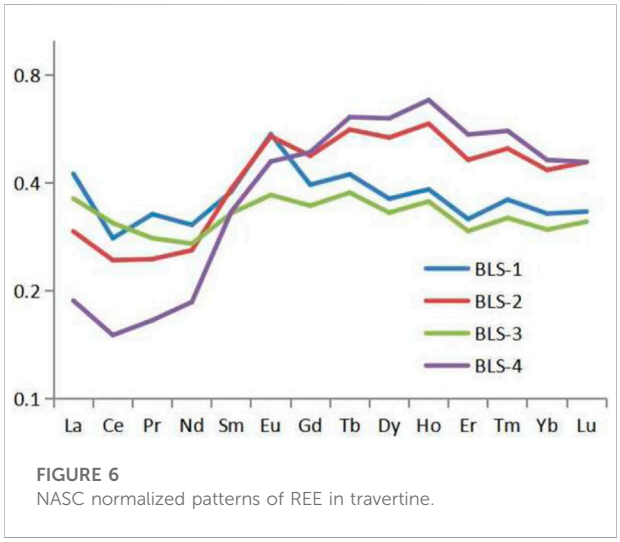

FIGURE 6
NASC normalized patterns of REE in travertine.

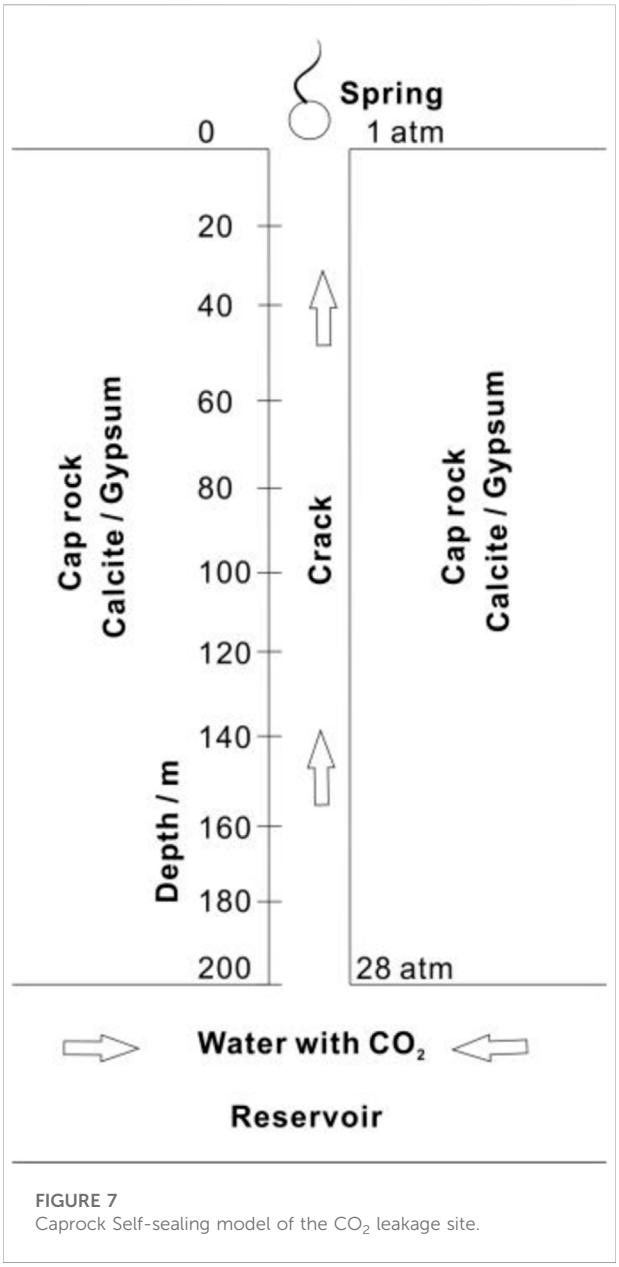

FIGURE 7
Caprock Self-sealing model of the CO_2 leakage site.

Numerical simulation results show that the CO_2-rich fluid migrates from the reservoir to the surface along the fracture, and the CO_2 partial pressure decreases in the process, resulting in the dissolution of gypsum and the precipitation of calcite in the fracture channel. During the process of migration to the surface, the dissolution and precipitation rates gradually increase. At the surface, 0.5644 g of gypsum can be dissolved per kilogram of fluid, and 0.9030 g of calcite can be precipitated. Set the density of gypsum to be 2.31 g/cm^3 and the density of calcite to be 2.71 g/cm^3. The volume of

TABLE 5 Main ionic components in groundwater.

Formation water composition	mg/L	Formation water composition	mg/L
Ca^{2+}	805	HCO_3^-	3,185
K^+	121	Cl^-	69.5
Mg^{2+}	165	SO_4^{2-}	908
Na^+	281	pH	7.28
Fe^{3+}	0.05	T	17

calcite precipitated during this process is larger than the volume of dissolved gypsum.

In the surface position, each liter of fluid can fill the gap up to 0.088881 cm^3, and in the 200 m deep crack, the gap can be filled by 0.04261 cm^3 per liter of fluid. The single-width flow rate of the fissure is set to be 2 L/s, and the top of the 0.3 m wide fissure is the first to complete self-sealing, which takes 390.66 days; and it took 814.89 days for the bottom of the fissure to finally complete self-sealing.

According to the flow monitoring of Bing Lingshan spring, the gas-liquid ratio of the fluid is about 0.8. It is speculated that when the 0.3 m-wide crack is completely self-sealing, the leakage of CO_2 from a single-width crack is about 140,813.3 m^3. Under the condition of 1 atm and a temperature of 25°C, the CO_2 density is 1.7845 kg/m^3, and the mass of CO_2 leaked from a single-width crack is about 251.28 tons.

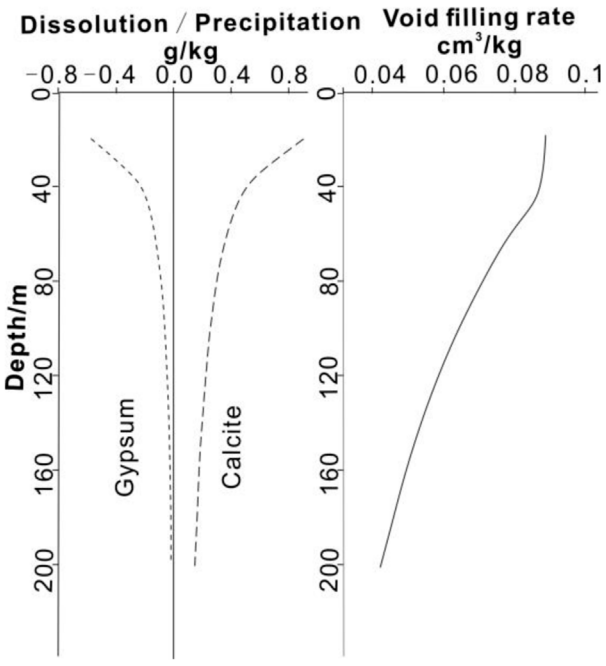

FIGURE 8
Mineral dissolution/precipitation and void filling rate variation curve with depth.

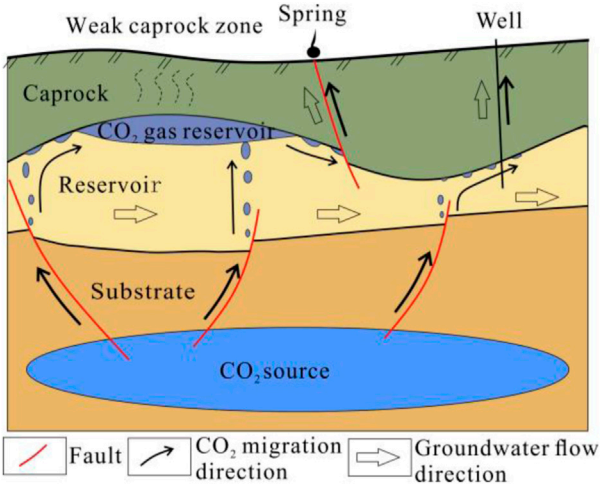

FIGURE 9
CO_2 leakage pattern diagram of Qinghai Ping'an.

Conclusion

1) The natural CO_2 leakage mechanism in Qinghai Ping'an is as follows: the deep carbonate minerals in the crust are decomposed at high temperature to generate CO_2, and the generated CO_2 rises into the reservoir along with the deep and large fault. Blocked by the caprock, CO_2 accumulates at the top of the reservoir, and then migrates to the leakage channel with the groundwater flow, and finally leaks to the surface.
2) Several vertical travertine veins can be seen in the section of the ancient travertine platform of Bing Lingshan in Ping'an County, Qinghai Province. They are formed by mineral precipitation from the CO_2-rich water in the water-conducting fissures, which confirms the existence of the self-sealing effect of the caprock. The microscopic morphology and geochemical characteristics show that the fractures have experienced 4 times of self-sealing, corresponding to four tectonic events.
3) Based on the hydrochemical analysis and geological observation data, the hydrogeochemistry numerical simulation was carried out. The results show that: first, gypsum dissolves and calcite precipitates during the migration of CO_2-rich water to the surface,

and the closer to the surface, the faster the dissolution and precipitation rate; 2nd, self-sealing occurs during the migration of CO_2-rich water to the surface, and the closer to the surface, the more significant the self-sealing effect is. The single-width flow rate of the fracture is set to 2 L/s. The top of the fracture is the first to complete self-sealing, which takes 390.66 days; and the bottom of the fracture is finally self-sealing, which takes 814.89 days; 3rd, according to the flow monitoring of Bing Lingshan spring, the gas-liquid ratio of the fluid is about 0.8. It is speculated that when the 0.3 m wide fissure achieves complete self-sealing, the leakage of CO_2 from a single wide fissure is about 140,813.3 m^3, or about 251.28 tons.

Data availability statement

The original contributions presented in the study are included in the article/supplementary material, further inquiries can be directed to the corresponding authors.

Author contributions

LF: Conceptualization, Methodology, Investigation, Funding acquisition. YD: Investigation, Writing—Original Draft. CZ: Resources, Methodology, Funding acquisition. XM: Software, Formal analysis, Visualization. TL: Supervision. XJ: Project administration. WS: Data Curation.

Funding

This research was funded by the, 2020 Qinghai Province "Kunlun Talents" Action Plan (青人才字[2020]18号), 2021 "High-level Talent Project" of Bureau of Geological Exploration and Development of Qinghai Province (青地矿科[2021]16号), Qinghai Province Science and Technology Application Basic Research Project under Grant No. 2022-ZJ-735, and China Geological Survey Project under Grant No. DD20221818.

Conflict of interest

The authors declare that the research was conducted in the absence of any commercial or financial relationships that could be construed as a potential conflict of interest.

Publisher's note

All claims expressed in this article are solely those of the authors and do not necessarily represent those of their affiliated organizations, or those of the publisher, the editors and the reviewers. Any product that may be evaluated in this article, or claim that may be made by its manufacturer, is not guaranteed or endorsed by the publisher.

References

Anelia, P., Adrian, C., Corinne, L., Martin, F., Noirez, S., Brichart, T., et al. (2021). Aquifer-CO_2 leak project: physicochemical characterization of the CO_2 leakage impact on a carbonate shallow freshwater aquifer-sciencedirect. *Int. J. Greenh. Gas Control* 106, 103231. doi:10.1016/j.ijggc.2020.103231

Choi, B. Y. (2019). Potential impact of leaking CO_2 gas and CO_2-rich fluids on shallow groundwater quality in the chungcheong region (South Korea): A hydrogeochemical approach[J]. *Int. J. Greenh. Gas Control* 84, 13–28. doi:10.1016/j.ijggc.2019.03.010

Cui, Zhendong, Liu, Da'an, Zeng, Rongshu, et al. (2011). Potential geological and environmental risks and its prevention measures for CO_2 geological storage projects. *Geol. Rev.* 57 (5), 700–706. (in Chinese with English abstract).

Delkhahi, B., Nassery, H. R., Vilarrasa, V., Alijani, F., and Ayora, C. (2020). Impacts of natural CO_2 leakage on groundwater chemistry of aquifers from the Hamadan Province, Iran. *Int. J. Greenh. Gas Control* 96, 103001. doi:10.1016/j.ijggc.2020.103001

Do, H. K., Yu, S., Ryuh, Y. G., Ju, Y., Kang, H. J., Ha, S. W., et al. (2022). Tracing CO2 leakage and migration using the hydrogeochemical tracers during a controlled CO_2 release field test. *Appl. Geochem.* 143, 105390. doi:10.1016/j.apgeochem.2022.105390

Erik, L., Per, B., Malin, T., and Grimstad, A. A. (2017). Aliso canyon leakage as an analogue for worst case CO_2 leakage and quantification of acceptable storage loss. *Energy Procedia* 114, 4279–4286. doi:10.1016/j.egypro.2017.03.1914

Fu, Lei, Zhang, S., Jia, X., Shengtao, Li., and Tao, Y. (2019). Test of the paleoenvironment reconstruction of bingling hill travertine in large time scale. *Quat. Sci.* 39 (2), 510–517. doi:10.11928/j.issn.1001-7410.2019.02.22

Gal, F., Proust, E., Humez, P., Braibant, G., Brach, M., Koch, F., et al. (2013). Inducing a CO_2 leak into a shallow aquifer (CO_2 Field Lab EUROGIA+project): Monitoring the CO_2 plume in groundwaters. *Energy Procedia* 37, 3583–3593. doi:10.1016/j.egypro.2013.06.251

Gale, J. (2004). Geological storage of CO_2: what do we know, where are the gaps and what more needs to be done? *Energy* 29, 1329–1338. doi:10.1016/j.energy.2004.03.068

Gupta, Pankaj Kumar, and Yadav, Basant (2020). Leakage of CO_2 from geological storage and its impacts on fresh soil–water systems: a review. *Environ. Sci. Pollut. Res.* 27, 12995–13018. doi:10.1007/s11356-020-08203-7

Ha, S. W., Park, B. H., Lee, S. H., and Lee, K. K. (2017). Experimental and numerical study on gaseous CO_2 leakage through shallow-depth layered porous medium: implication for leakage detection monitoring. *Energy Procedia* 114, 3033–3039. doi:10.1016/j.egypro.2017.03.1431

Jefferson, M. (2015). IPCC fifth assessment synthesis report: "climate change 2014: longer report": critical analysis. *Technol. Forecast. Soc. Change* 92 (3), 362–363. doi:10.1016/j.techfore.2014.12.002

Johnson, G., Hicks, N., Bond, C. E., Gilfillan, S., Jones, D., Kremer, Y., et al. (2017). Detection and understanding of natural CO_2 releases in KwaZulu-Natal, South Africa. *Energy Procedia* 114, 3757–3763. doi:10.1016/j.egypro.2017.03.1505

Jonathan, P., Dave, J., Jerry, B., Beaubien, S., Foekema, E., Gemeni, V., et al. (2014). A guide for assessing the potential impacts on ecosystems of leakage from CO_2 storage sites. *Energy Procedia* 63, 3242–3252. doi:10.1016/j.egypro.2014.11.351

Jones, D. G., Barkwitha, A. K. A. P., Hannis, S., Lister, T., Gal, F., Graziani, S., et al. (2014). Monitoring of near surface gas seepage from a shallow injection experiment at the CO_2 Field Lab, Norway-ScienceDirect. *Int. J. Greenh. Gas Control* 28 (2), 300–317. doi:10.1016/j.ijggc.2014.06.021

Karas, D., Demić, I., Kultysheva, K., Antropov, A., Blagojevic, M., Neele, F., et al. (2016). First field example of remediation of unwanted migration from a natural CO_2 reservoir: the bečej field, Serbia. *Energy Procedia* 86, 69–78. doi:10.1016/j.egypro.2016.01.008

Li, Xiaochun, Hitoshi, Koide, and Takashi, Ohsumi (2003). CO_2 aquifer storage and the related rock mechanics issues. *Chin. J. Rock Mech. Eng.* 22 (6), 989–994. (in Chinese with English abstract).

Ma, D., Gao, J., Gao, Z., Jiang, H., Zhang, Z., and Xie, J. (2020). Gas leakage recognition for CO_2 geological sequestration based on the time series neural network-ScienceDirect. *Chin. J. Chem. Eng.* 28 (9), 2343–2357. doi:10.1016/j.cjche.2020.06.014

Mark, L. P., Michael, P., Rajesh, P., and Illangasekare, T. (2014). CO_2 leakage into shallow aquifers: modeling CO_2 gas evolution and accumulation at interfaces of heterogeneity. *Energy Procedia* 63, 3253–3260. doi:10.1016/j.egypro.2014.11.352

Melis, C., Jonathan, M. B., Mark, E. V., Gernon, T. M., Wright, I. C., and Long, D. (2015). Gas migration pathways, controlling mechanisms and changes in sediment acoustic properties observed in a controlled sub-seabed CO_2 release experiment. *Int. J. Greenh. Gas Control* 38, 26–43. doi:10.1016/j.ijggc.2015.03.005

Qafoku, N. P., Lawter, A. R., Bacon, D. H., Zheng, L., Kyle, J., and Brown, C. F. (2017). Review of the impacts of leaking CO_2 gas and brine on groundwater quality. *Earth-Science Rev.* 169, 69–84. doi:10.1016/j.earscirev.2017.04.010

Ren, S., Li, D., Zhang, L., and Huang, H. (2014). Leakage pathways and risk analysis of CO_2 in geologic storage. *Acta Pet. Sin.* 35 (3), 591–601. (in Chinese with English abstract). doi:10.7623/syxb201403024

Roberts, J. J., Laplastrier, A., Shipton, Z. K., Bell, A. F., and Karolyte, R. (2019). Structural controls on the location and distribution of CO_2 emission at a natural CO_2 spring in Daylesford, Australia. *Int. J. Greenh. Gas Control* 84, 36–46. doi:10.1016/j.ijggc.2019.03.003

Saleem, U., Dewar, M., Tariq, N. C., Sana, M., Lichtschlag, A., Alendal, G., et al. (2021). Numerical modelling of CO2 migration in heterogeneous sediments and leakage scenario for STEMM-CCS field experiments. *Int. J. Greenh. Gas Control* 109, 103339. doi:10.1016/j.ijggc.2021.103339

Schroder, I. F., Wilson, P., Feitz, A. F., and Ennis-King, J. (2017). Evaluating the performance of soil flux surveys and inversion methods for quantification of CO_2 leakage. *Energy Procedia* 114, 3679–3694. doi:10.1016/j.egypro.2017.03.1499

Susan, A. C., Elizabeth, K., Kayyum, M., Dai, Z., Sun, Y., Trainor-Guitton, W., et al. (2014). Key factors for determining groundwater impacts due to leakage from geologic carbon sequestration reservoirs. *Int. J. Greenh. Gas Control* 29, 153–168. doi:10.1016/j.ijggc.2014.07.007

Taylor, Peter, Stahl, H., Toberman, M., Sayer, M. D., Reynolds, A., Sato, T., et al. (2015). Impact and recovery of pH in marine sediments subject to a temporary CO_2 leak. *Int. J. Greenh. Gas Control* 38, 93–101. doi:10.1016/j.ijggc.2014.09.006

Vialle, S., Druhan, J. L., and Maher, K. (2016). Multi-phase flow simulation of CO_2 leakage through a fractured caprock in response to mitigation strategies. *Int. J. Greenh. Gas Control* 44, 11–25. doi:10.1016/j.ijggc.2015.10.007

Xiao, T., Wang, B., Xu, L., Esser, R., Dai, Z., Cather, M., et al. (2022). Underground sources of drinking water chemistry changes in response to potential CO_2 leakage. *Sci. Total Environ.* 847, 157254. doi:10.1016/j.scitotenv.2022.157254

Xie, Jian, Ning, Wei, Wu, Zhouli, et al. (2017). Progress in leakage study of geological CO_2 storage. *Rock Soil Mech.* 38, 181–188. doi:10.16285/j.rsm.2017.S1.021

Xu, Zhigang, Chen, Daizhao, and Zeng, Rongshu (2008). The leakage risk assessment and remediation options of CO_2 geological storage. *Geol. Rev.* 54 (3), 373. doi:10.16509/j.georeview.2008.03.014

Zahasky, C., and Benson, S. M. (2016). Evaluation of hydraulic controls for leakage intervention in carbon storage reservoirs. *Int. J. Greenh. Gas Control* 47, 86–100. doi:10.1016/j.ijggc.2016.01.035

Zhai, X., Ge, H., Chen, X., Xu, Y., and Fan, G. (2018). The influence of CO_2 leaking on environmental monitoring in the process of CO_2 geological sealing. *Energy Procedia* 153, 207–214. doi:10.1016/j.egypro.2018.10.034

Zhao, X., Deng, H., Wang, W., Han, F., Li, C., Zhang, H., et al. (2017). Impact of naturally leaking CO_2 on soil properties and ecosystems in the Qinghai-Tibet plateau. *Sci. Rep.* 7, 3001. doi:10.1038/s41598-017-02500-x